Crystal Nucleation, Growth and Morphology of the Synthetic Malaria Pigment β-Hematin and the Effect Thereon by Quinoline Additives: The Malaria Pigment as a Target of Various Antimalarial Drugs

Inna Solomonov,[†] *Maria Osipova*,[†] *Yishay Feldman*,[‡] *Carsten Baehtz*,[§] *Kristian Kjaer*,[£] *Ian K. Robinson*,[#] *Grant T. Webster*,[††] *Don McNaughton*,[††] *Bayden R. Wood*,[††] *Isabelle Weissbuch*,[*†] *Leslie Leiserowitz*[*†]

[†]Dept. of Materials and Interfaces, The Weizmann Institute of Science, 76100-Rehovot, Israel;

[‡]Chemical Research Support, The Weizmann Institute of Science, 76100-Rehovot, Israel;

[§]Hasylab at DESY, Notkestr. 85, D-22607 Hamburg, Germany;

[£]Niels Bohr Institute, University of Copenhagen, Universitetsparken 5, DK-2100 Copenhagen, Denmark;

[#]Dept. of Physics and London Centre for Nanotechnology, University College, Gower St, London WC1E 6BT, England;

[††]Centre for Biospectroscopy and School of Chemistry, Monash University, 3800, Victoria, Australia.

Supporting Information

Experimental Section

Preparation of β-hematin crystals. β-Hematin crystals were grown using a standard and reliable way of obtaining β-hematin from a MeOH-DMSO solution containing hemin (Chloro(protoporphyrinato)iron(III) or Ferriprotoporphyrin IX chloride, Sigma) and 2,6-lutidine (2,6-dimethylpyridine) base.[27] In order to adopt the above procedure of crystal formation in the bulk to the

air-water interface, we replaced MeOH-DMSO by chloroform. In the first procedure 0.489g of hemin was dissolved in a minimal amount of dry 2,6-lutidine with stirring. Upon completion of the dissolution a 1:1 (35:35mL) mixture of MeOH and DMSO was added and the flask sealed and protected from moisture and ambient light. Such flasks were allowed to stand undisturbed from a few hours to several months. After an allotted time, the solution was filtered and a black precipitate collected, which was then washed with 50 mL MeOH and with deionized water until decanted water layers were colorless. The solid was dried in a dessicator until made use of.

For the second method of β-hematin preparation, ~3mg of hemin was dissolved in dry 2,6-lutidine (about 0.5mL), sonicated for 5min to form a homogenuous solution, to which chloroform was added to yield a 10 mL solution. After keeping the solution in the dark for 12 hours a black precipitate of β-hematin was formed.

For the induced nucleation of β-hematin crystals by a monolayer of dibehenoyl-*L*-α-phosphatidylcholine (DBPC) transferred on a octadecyltrichlorosilane (OTS)-covered Si wafers, the latter were placed vertically in the chloroform solution. The OTS monolayer on the surface of a Si (111) wafer was prepared according to the following procedure: (i) wafer sonication in acetone for 15 min; (ii) removal of the native SiO_2 layer in 40% NH_4F solution for 1 hour; (iii) sonication in Millipore water for 15 min; (iv) growing a fresh oxide layer in piranha solution (2:1 v of 96% H_2SO_4: 30% H_2O_2) at 90-100 ºC for 30 min.; (v) sonication in water for 15 min and drying with pure N_2; (vi) immersion in a solution of OTS in bicyclohexyl ($2*10^{-2}$ M) for 24 hours followed by sonication for 15 min. in CCl_4, toluene, ethanol and water and drying with pure N_2. The average thickness of the OTS monolayer was found to be 29±4Å, by ellipsometry. A contact angle of 70º attests to the hydrophobic nature of the OTS-Si wafer. A monolayer of the phospholipid DBPC was compressed 30 mN/m on the water surface of a Langmuir trough and transferred by the Langmuir-Schaffer technique onto the OTS-Si wafer.

X-ray powder diffraction of hematin crystals nucleated by the DBPC monolayer. The measurements were carried out in reflection mode using a TTRAX III (Rigaku) diffractometer equipped

with a rotating anode Cu anode operating at 50 kV and 240 mA. First, specular diffraction (θ/2θ scan) that probes only crystallographic planes parallel to the plane of the Si wafer was made in Bragg-Brentano geometry. Then pole figures of the strong reflections were recorded at fixed Bragg angles using a Multi-purpose Attachment III (Euler cradle) that performed in-plane sample rotation at regularly increasing sample's tilt with respect to incident/diffracted beams plane.

Transmission Electron Microscopy (TEM) Measurements. The crystalline powders of β-hematin were dispersed in water and a drop deposited onto specimen grids (SPI, Cu 300 mesh) coated with carbon (upper) and polymer films. Selected specimen crystals were characterized in a TEM Philips CM120 microscope operated at 120 kV. Care was taken to minimize the time of beam irradiation received by each specimen during its imaging since crystal damage by the electron beam was sometimes observed. Electron diffraction (ED) patterns of single crystals were obtained from various specimens by selected area ED and their *d*-spacings measured with an accuracy of ±0.005 nm, using Gold and asbestos ED patterns as reference standards.

Grazing Incidence X-ray Diffraction (GIXD) Measurements. Chloroform solutions of hemin and 2,6-lutidine were spread at the air-water interface for the GIXD measurements, which were performed on the liquid surface diffractometer at the BW1 undulator beamline at the HASYLAB synchrotron source at DESY, Hamburg. The solutions were spread at room temperature on the water surface in a Langmuir trough. The air surrounding the trough was replaced by helium to reduce X-ray background scattering. The X-ray diffraction measurements were performed upon cooling the water subphase to 5°C. A monochromatic X-ray beam (λ=1.304Å) was adjusted to strike the liquid surface at an incident angle $\alpha_i < 0.85\alpha_c$ where α_c is the critical angle for total external reflection; this maximizes surface sensitivity. The GIXD signals are obtained from thin film crystallites that are randomly oriented about the water surface normal in the form of a 2D "powder". A detailed description of GIXD applied to films on liquid surfaces has been given elsewhere.[20,22-24]

Synchrotron Powder X-ray Diffraction. The experiments were performed on a powder X-ray

diffractometer[32] at beamline B2 located at a bending magnet of the storage ring DORIS at HASYLAB, Hamburg. For monochromatisation, a water-cooled Si (111) double flat-crystal monochromator is used. A Ge (111) analyzing crystal in front of a scintillation counter allows collection of well-resolved powder diffraction data with a high signal-to-noise ratio. The samples, which -- in order to avoid affecting crystal coherence -- were not milled, were filled in glass capillaries with an outer diameter of 0.9 mm and a wall thickness of 0.01mm. The wavelengths of the synchrotron radiation used were 0.4528, 0.47 and 0.4996Å. The measurements were carried out at room temperature; a step size of 0.003° was chosen and the time for data collection was between 12 and 15h. In general the full width at half maximum (FWHM) of a reference material (LaB_6, 660a NIST standard) is $2\theta \approx 0.007°$ with the setup, measured with a step size of 0.001°.

Coherent Grazing Exit X-ray Scattering. To examine the morphology of the crystal grains, Coherent X-ray Diffraction (CXD) experiments were undertaken at the 34-ID-C beamline of the Advanced Photon Source, Argonne National Laboratory, USA. The geometry used was similar to the coherent grazing exit scattering geometry for probing the structure of thin films[30], except that the detector was set to the Bragg angle of one of the strong powder reflections. The incident beam was focused to about 1 micron to limit the number of grains illuminated. Searches of the sample position and angle were made until the diffraction from a single grain was centered on the detector. The 2D direct-detection charge-coupled device (CCD) X-ray detector with a 20-micron pixel size was placed 1m from the sample to record the detailed sample of the Bragg reflection.

IR Attenuated Total Reflectance (ATR) spectroscopy. IR-ATR hyperspectral images were collected ($6cm^{-1}$ resolution and 64 co-added scans) on a Varian Stingray imaging spectrometer (Varian inc, US), equipped with a 64 × 64 MCT Focal Plane Array (FPA) detector and a Ge ATR objective. The large refractive index of the Ge objective allows sub diffraction limit spectroscopy, providing a spatial resolution that is almost as good as the Raman microscope[33,34]. The depth penetration of the IR-ATR is wavelength dependent and approximately equal to the wavelength of the radiation (*ca* 5-10 μm for the

wavenumber region of interest) so for infrared images the spectrum associated with each "pixel" is of a number of crystals. The Raman spectra, in contrast, are of individual crystals. The Ge objective was lowered on to β-hematin crystals on a microscope slide until sufficient pressure was applied to obtain adequate S/N. The hyperspectral images thus provided 4096 spectra of β-hematin, and quinine/chloroquine treated β-hematin. Spectral images were analyzed using the Cytospec software (Cytospec inc, NY, USA).

Micro-Raman Imaging Spectroscopy. Raman spectra were acquired on a Renishaw micro-Raman system 2000 (Renishaw pty ltd, Wootton-under-edge, UK) using 830nm excitation and a ×60 water immersible objective. Single crystals in a flat orientation were targeted. Spectra of 17 crystals of β-hematin and 16 crystals of β-hematin, grown in the presence of quinine and chloroquine, were recorded. Principal Components Analysis (PCA) within Unscrambler (Camo, Norway) was used to analyze the dataset. Each spectrum was recorded in 10 seconds with a *ca* 1-2 μm laser spot size and approximately 2-3 mW power on the sample.

Figure S1. Reported effect of carbon chain length on the antimalarial activity (IC_{50}) and heme affinity (K_a) of diethylamino-hydroxyxanthone molecules[13].

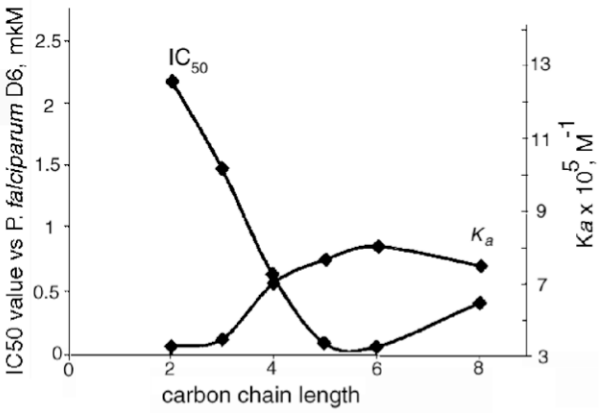

Inhibition of Crystal Nucleation of *R,S*-Mandelic Acid with Quinine. It is noteworthy that quinoline additives may inhibit the nucleation and growth of carboxylic acid crystals. For example, the crystal

precipitation time of *R,S*-mandelic acid increases significantly in the presence of 2.5% quinine and the crystals grow at a much slower rate (Table S1) although they do not change their shape relative to that of the pure form (Figure S2c).

Table S1. Visual inspection and estimate of the percentage of surface covered with crystal bunches of *R,S*-mandelic acid after the solution was poured in Petri dishes, cooled to RT and one single crystal seed inserted into each dish. (Q denotes additive quinine)

Time hrs	4g/10mL H_2O 6 exp.	4g/10mL H_2O 2.5%mol Q 3 exp.	4g/10mL H_2O 1%mol Q 6 exp.	4.5g/10mL H_2O 1.0%mol Q 6 exp.	4.5g/10mL H_2O 0.5%mol Q 6 exp.
0.5	fully crystallized	seed	seed	seed	few bunches
1.0		seed	seed	few bunches	~20%
1.5		seed	few bunches	~20-30%	~40%
2.0		seed+2 crystals	~50%	~50%	70-80%
4.0		few bunches	fully crystallized	70-80%	fully crystallized

This behavior may be understood in terms of the crystal structure of *R,S*-mandelic acid[52]; quinine should be able to inhibit growth of the eight symmetry-related {111} side faces as well as the {010} plate-like faces crystal, from which the carboxyl groups emerge (Figure S2a, b).

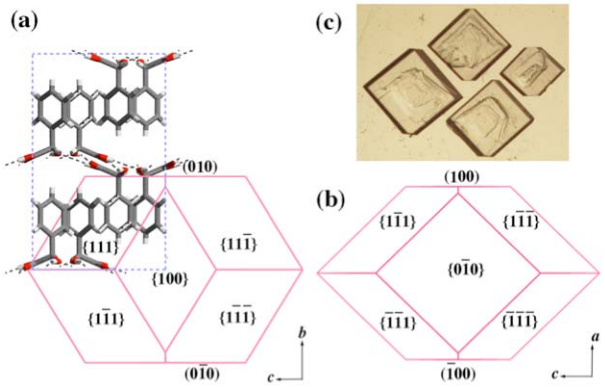

Figure S2. (a) Part of crystalline packing arrangement of *R,S*-mandelic acid. (b) Theoretical growth morphology depicting the various faces. (c) Photographs of {010} plate-like crystals of *R,S*-mandelic acid obtained from solution.

Binding of Diethylamino-alkoxyxanthones on β-Hematin Crystal Faces and Antimalarial Activity. In the Introduction, we alluded to the antimalarial activity of the diethylamino-alkoxyxanthones (Formula 1, main text), labeled XN*n*, *n* = 2-8, as expressed by a strong correlation, shown in SI Figure S1, between the heme affinity (*Ka*) measured in aqueous solution, the chain length and antimalarial potency as measured by the inhibitory concentration IC_{50} values[13]. Here we compare, by computation, the relative ability of XN*n* molecules with $(CH_2)_n$ side chains, *n*=2 (XN2) and *n*=5 (XN5), which have distinctly different IC_{50} values (2.2 *vs* 0.1 μM), to bind to the {011} and {001} crystal surfaces of β-hematin.

The drug has at each opposite end of the molecular chain an amino group that may bind to a surface-exposed β-hematin propionic acid moiety, via an $N\text{-}H^{+\cdots}OOC$ interaction. The presence of an amine group at each end of the drug should, in principle, produce a stronger binding than a single amine group provided both ends are linked to the crystal surface by $N\text{-}H^{+\cdots}O_2C$ hydrogen bonds. Such simultaneous binding would constitute more efficient "surface capping"[48] and subsequent crystal growth inhibition, leading to increased antimalarial efficiency of the drug. We confined the computational search of possible surface binding sites to those that would not only allow both amino groups of the drug to participate in hydrogen bonds, but also permit the formation of favorable van der Waals contacts between the crystal surface and the drug along its length. This constraint limited the search. The CERIUS[2] (Accelrys) software package was made use of for modeling the docking of the drug onto the {001} and {011} crystal surfaces and for eventual energy minimization of the system.

The length of molecule XN2 in extended form is ~17Å and thus too long to effectively bind to two carboxyl groups separated by the axial distance a = 12.2Å, but too short to bind to two such groups separated by 2a. Nevertheless, the molecule can align itself on the {001} face along the a axis and form an acid-base $NH^+\ldots{}^-O_2C$ bond at one end and a weaker $NH^+\ldots$ O=C-(Fe) interaction at its opposite end (Figure 13c,d). The computed docking energy is ~ -25 kcal/mol (Table 2).

Although we find a clear-cut correlation between the computed docking energies and the experimental IC_{50} values, other factors obviously may be at play. For example, molecule XN5, being longer than XN2, will induce a greater distortion about its immediate crystalline environment during the deposition of oncoming β-hematin molecular layers and so will be a stronger inhibitor to further growth and thus be a more effective antimalarial. Furthermore, we note that the smooth {100} face may also be a suitable $NH^{+\cdots-}O_2C$ binding substrate for XN additives even though the face exposes carboxyl groups at an oblique angle to the surface, yet which are conformationally flexible (Figure 1b). Once again XN5 has the advantage that it can bind to the {100} face in more ways than XN2.

Model Study of Inhibition of Crystal Nucleation of *S*-alanine via Additive Combinations. We made use of *S*-alanine (*S*-Ala) as the host crystal, which consists of H-bonded chains aligned parallel to the *c*-axis (Figure S3a). The crystals, grown under ambient conditions from aqueous solutions of concentration 25g/100mL, were obtained after about 15-20 min (Figure S3b). *S*-Ala crystals grown in the presence of 1% *S*-phenylalanine (Phe) appeared after two hours as [001] needles (Figure S3e), a change in habit due to binding *S*-Phe to the crystal side faces (Figure S3d). Retardation of growth in the *c*-direction was attempted using three diamines, *o*- and *p*-phenylenediamines (labeled OPD and PPD) and 1,6-diaminohexane (DAH), the idea being that the amino groups would H-bond to the carboxylate groups exposed at the {011} faces of *S*-ala. The presence of 10% of each in the solution did not change the crystal habit, yet did delay precipitation time. The solution containing OPD and PPD yielded crystals within half an hour and two hours respectively, DAH delayed crystallization for 2-4 hours (based on 27 experiments). We propose that DAH is the better retarder of crystal nucleation because of chain flexibility and a molecular length (6.4Å) that matches the distance of 6Å between carboxylate groups on the {011} face (Figure S3f). A cocktail of 1% *S*-Phe and 10% DAH delayed appearance of *S*-Ala crystals from 8-20 hours, indicating that simultaneous use of two types of additives, which bind to different crystal faces, has a greater inhibiting effect on nucleation than each of the additives used alone.

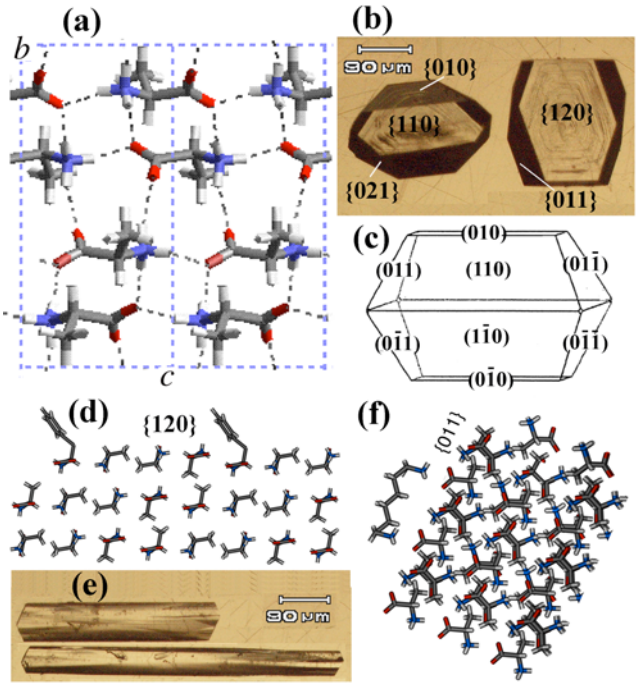

Figure S3. (a) Molecular packing arrangement of crystalline *S*-ala. (b) Photographs of the two different morphologies obtained from aqueous solution. The crystals faces are indexed. (c) Theoretical growth morphology. (d) Edge-on view of a {120} face of *S*-ala crystal, showing additive *S* Phe adsorbed thereon. (e) Morphology of *S*-ala crystals grown in the presence of additive *S* Phe. (f) Edge-on view of a {011} face of *S*-ala crystal, showing additive 1,6-diaminohexane (DAH) adsorbed thereon.